Electrochemical Study of the Corrosion Performance of AISI-309 and AISI-310 Exposed in NaVO$_3$ at High Temperature

O. Sotelo-Mazón[1], C. Cuevas-Arteaga[1,*], J. Porcayo-Calderón[1], Rosa Ma. Melgoza-Alemán[1], Ma. G. Valladares Cisneros[1], G. Izquierdo-Montalvo[2], L. Martínez Gómez[3,4].

[1] FCQeI-CIICAp-Universidad Autónoma del Estado de Morelos, Av. Universidad 1001, Col. Chamilpa, C.P. 62210, Cuernavaca, Morelos, México.
[2] Instituto de Investigaciones Eléctricas, Reforma 113, Col. Palmira, C.P. 62490, Cuernavaca, Morelos, México.
[3] Instituto de Ciencias Físicas, Universidad Nacional Autónoma de México, Avenida Universidad s/n, 62210, Cuernavaca, Morelos, México.
[4] Corrosión y Protección (CyP), Buffon 46, 11590 México City, DF, México
*E-mail: ccuevas@uaem.mx

Corrosion performance of AISI-309 and AISI-310 exposed in NaVO$_3$ at 700°C was studied using some electrochemical techniques named potentiodynamic polarization measurements and linear polarization resistance (Lp). Measurements of potential in time and mass loss were also obtained. From the physical characterization, it was observed a similar corrosion mechanism for both materials, determining the formation of three different corrosion products layers, which consisted in a concentrated NiO inner layer, a combined layer of Cr$_2$O$_3$-Fe$_2$O$_3$-NiO$_2$, and the molten salt chemically associated with chromium and iron as FeVO$_4$ and CrVO$_4$. Both stainless steels presented a similar type of corrosion attack, a generalized mixed corrosion along the surface, stating that the difference in composition of the two stainless steels seems not to have a relevant significance in the corrosion mechanism. From the electrochemical techniques, it was determined that AISI-310 has a lightly better corrosion performance respect to AISI-309, since its corrosion potential was nobler and the corrosion rate was smaller. The electrochemical and weigh loss data obtained in this study have provided consistent information in order to evaluate the probable use of these stainless steels in applications where the fuel in industrial furnaces is a residual oil containing the species vanadium.

1. INTRODUCTION

The power generation systems, which use residual fuel oil for their needs in the production of vapor, suffer important high temperature corrosion by molten salt in the furnaces, having significant

economic losses. The corrosion problems together with the deformation of the metallic materials limit the vapor temperature, leading to a low efficiency in the power generation and therefore in the production of electricity [1]. The use of fuel oil in the power generation industry started in 1920, since then, the presence of ash deposits has been observed in the gas side of the furnaces. The nature and their significance of such deposits in the corrosion processes depend on the type of fuel oils and their impurities [2]. The contamination of the external surfaces of superheaters or reheaters with ashes having a high concentration of elements such as vanadium, sodium and sulphur, mainly as Na_2SO_4-V_2O_5 complex mixtures and sodium–vanadates compounds are generated during the combustion processes of residual fuel oil [3,4,5], becoming in a concern between 1940 and 1950, since during these years the vapor temperature increased and the fuel oil heightened its content of vanadium. Some investigations have also reported that the three main found elements in the residual fuel oils are sodium, chlorine and vanadium, in concentrations greater than 100 ppm. In addition, iron and nickel could be present at 25 ppm, whereas the sulfur could be present up 3% [3]. However, just 50 ppm of vanadium can be enough to produce a very serious corrosion problem [6]. During the combustion, vanadium is present as gaseous compounds like oxides or hydroxides. The gaseous combustion products are probably VO and VO_2 [7,8], whose proportion is determined by the amount of oxygen absorbed from the atmosphere. Nevertheless, these vanadium oxides have a very low saturated vapor pressure, which means that condense over the heat metallic surfaces of superheater or reheaters [9]. The species V_2O_5 will be formed once the gases are cooled and oxygen is absorbed [10-13] Once V_2O_5 is formed, the chemical interaction of this oxide with the gaseous species NaCl and NaOH is highly probable, producing $NaVO_3$, with water and hydrochloric acid as secondary products [14, 15].

By the other hand, the compositions of the ashes in the deposits have been studied and reported [15]. The findings of this studies indicated that vanadium compounds were initially deposited over the external superheaters and reheaters surfaces as insoluble vanadium pentoxide (V_2O_5), and then reacted with sodium sulphate (Na_2SO_4) at 620°C forming $NaVO_3$ and sulfur trioxide. The formation of $NaVO_3$ whose molten point is 630°C, is greatly probable when residual fuel oil is used in the industrial furnaces, whereas the melting point of V_2O_5 is 690°C, which means that even though $NaVO_3$ is less acidic than V_2O_5, it is more volatile, therefore the heat metallic surfaces will be covered firstly with $NaVO_3$. In fact, a very complex mixture of vanadates and sulfates are present as ashes of the combustion of the residual fuel oil over the metallic surfaces, being the vanadates those of the lower melting points. So that, metallic surfaces at temperatures higher than 650°C will surely be subjected to corrosion due to vanadium attack. It is important to mention that as far as the authors know, there are very few reported studies related to the corrosion attack in $NaVO_3$ molten salt, so, this research constitutes a contribution in the corrosion mechanism and corrosion resistance of candidate materials to be used in combustion equipment where residual fuel oil is consumed leading to keep metallic surfaces at high temperature up 650°C. Vanadium is chemically very active at 650°C, producing several complex compounds, which allow an important vanadium attack of the metallic surfaces [4].

Accordingly to the above described, and in order to contribute in the material selection as one of the ways to deal with the corrosion problems, in this work it is presented the study of two candidate and accessible materials such as AISI-309 and AISI-310 exposed to $NaVO_3$ at 700°C. This study was made using two electrochemical techniques: potentiodynamic polarization and linear polarization

resistance. The mass loss from the conventional weight loss method and the open circuit potential in time were also utilized as experimental evidences to propose the corrosion mechanism. Some superficial and corrosion products characterization techniques such as SEM and DRX were used, whose results supported the electrochemical behavior.

2. MATERIALS AND METHODS

The specimens were cut and obtained from a bar of AISI-309 and AISI-310, which composition is presented in Table 1. The specimens consisted in rectangular parallelepipeds whose size was 10x5x5 mm, which were ground with silicon carbide sandpaper up 600 grit, washed in an ultrasonic bath with ethyl alcohol and dried under a warm air stream.

The specimens were spot welded to 80Cr-20Ni (wt. %) wire, which was used as electrical connection with the potentiostat/galvanostat. To avoid the corrosion of the 80Cr-20Ni wire in contact with the molten salt, the wire was introduced into a ceramic tube. Refractory cement was put into the wire and the ceramic tube. 500 mg/cm^2 of $NaVO_3$ (analytical regent) were introduced into a 30 ml silica crucible, which was set inside an electrical tube furnace to reach the temperature of 700°C ± 3°C. During the molten salt corrosion processes, the metallic surfaces are usually exposed in a thin molten salt film together with a gas mixture of O_2, SO_2, SO_3, whereas the experimental procedure performed in this research was made in bulk melt tests with static air.

Table I. Chemical elemental composition of the studied stainless steels.

Alloy Based Fe	Composition (Weight %)				
	Cr	Ni	C	Mn	Si
309	23.0	13.5	0.2	2.0	0.75
310	24.0 -26.0	19.0- 22.0	0.08	2.0	1.00

For the two polarization techniques, the electrochemical cell was formed by the working electrode and two 1 mm diameter platinum wires as auxiliary and reference electrodes. The platinum wires were treated as the 80Cr-20Ni wires, leaving 5 mm long free to contact with the molten salt. This reference electrode has been used widely, under similar molten salt conditions [16-18]. The stationary conditions of the corrosive system was reached after 20 min of immersion of the three electrodes in the molten salt. The anodic and cathodic measurements were obtained polarizing the specimen from -400 mV to +1500 mV with respect to the E_{corr} at a scan rate of 1 mV/s. The selection of this scan rate has been previously published elsewhere [19]. The linear polarization data were obtained applying ±20 mV at a scan rate of 10 mV/min during 100 hours. All the Electrochemical measurements were made using an ACM Instruments Auto DC potentiostat controlled by a personal computer.

In order to explore the corrosion performance of the studied materials beyond 100 h, the weight-loss method was applied until 250 h obtaining the mass loss each 50 hours, using different

specimens for each measurement. The procedure was made according to ASTM Standards G1 and G31 [20-21]. Each specimens was immersed in the molten salt inside a silica 30 ml crucible under the same experimental conditions than the electrochemical test. The type of corrosion attack of the AISI-309 and the AISI-310 was obtained after observing the free corrosion products specimens through SEM. The morphology and distribution of reaction products over the surface was obtained from the working electrode without de-scaling from the Lp technique using a Microspec WDX-3PC system connected to a Zeiss DSM960 scanning electron microscope. The corrosion products were analyzed using a Siemens D-500 Diffractometer operating with Cu Kα radiation. The XRD spectra were interpreted using the Powder Diffraction Data File reference [22].

3. RESULTS AND DISCUSSION

3.1 Physical Characterization

Figure 1 presents a micrograph and mappings of Fe, Cr, Ni, Mn, O, V and Na of the substrate-corrosion products interface of the corroded AISI-309 exposed to $NaVO_3$ at 700°C during 100 h from Lp. Through the micrograph, two interfaces are distinguished: the metallic surface/oxides and the metallic oxides/molten salt. The mappings of Fe, Cr and Ni show the presence of approximately 40 μm of chromium and iron oxides, and in much less extent nickel oxide, since, they are related with oxygen, accordingly to the corresponding mapping.
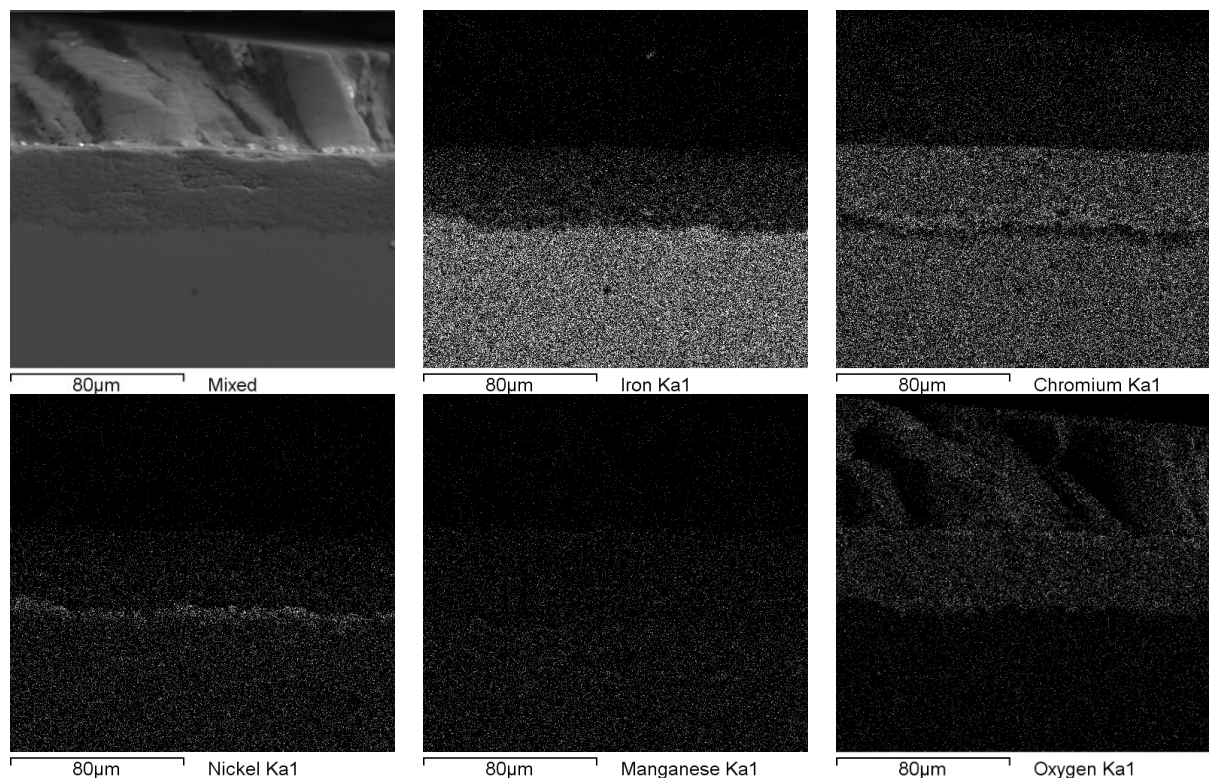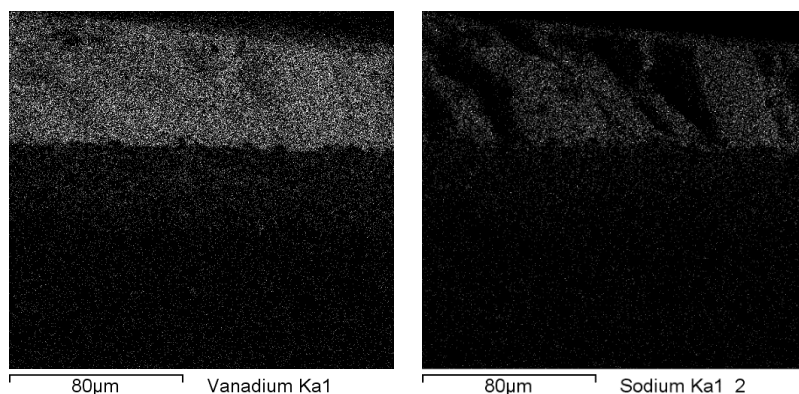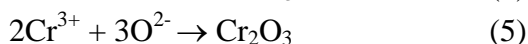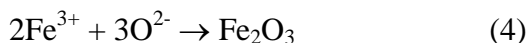
Figure 1. Image of the metal-corrosion products interface and X-ray mappings of Fe, Cr, Ni, Mn, O, V and Na of AISI-309 exposed to $NaVO_3$ at 700°C during 100 h from Lp technique.

The iron layer is less dense than that for chromium, which confirms that Cr is the alloy element that protects best the materials under certain experimental conditions. Also, a light layer of porous chromium oxide is observed above the denser and apparently non-dissolved Cr_2O_3. This porous layer is related with oxygen, vanadium and sodium, as an evidence of the possible formation of secondary corrosion products by means of chemical reactions between these four species. A much lighter porous iron layer is also seen in combination with the dissolved porous Cr_2O_3 layer, no evidence of nickel is seen together with the porous chromium and iron layer. Below the dense and non-dissolved Cr_2O_3 layer, there is a 4 μm thin and non-totally continuous nickel layer, which is just in the interface metallic surface/oxides. From the above observations, it seems that the AISI-309 formed a combined oxide layer constituted by NiO, Fe_2O_3 and especially with Cr_2O_3 as the protective, compact and coherent oxide layer, in spite of a major dissolution of chromium was seen, such as it has been reported elsewhere [23-25]. With respect to manganese, there is no evidence of some effect over the corrosion mechanism, which is due to composition of this element in the alloy is only 2 wt. %. The growth of the oxide layers is due to the ionization of metallic atoms present in the alloy through the oxidation reactions in presence of the corrosive medium, forming the metallic ions Fe^{3+}, Ni^{2+} and Cr^{3+}, which react with oxygen accordingly to the next reactions:

$$Fe \rightarrow Fe^{3+} + 3e^- \qquad (1)$$
$$Cr \rightarrow Cr^{3+} + 3e^- \qquad (2)$$
$$Ni \rightarrow Ni^{2+} + 2e^- \qquad (3)$$

Afterward, the formation of the metallic oxides is given through the next secondary reactions:

$$2Fe^{3+} + 3O^{2-} \rightarrow Fe_2O_3 \qquad (4)$$
$$2Cr^{3+} + 3O^{2-} \rightarrow Cr_2O_3 \qquad (5)$$
$$Ni^{2+} + O^{2-} \rightarrow NiO \qquad (6)$$

As a result, the concentration of oxygen over the metallic surface increases, which improves the diffusion of oxygen to the alloy to continue the formation of metallic oxides. Also, it has been stablished that vanadates compounds such as $NaVO_3$ are good oxidation catalyst and oxygen carriers to the metallic Surface [18]. In addition, in order to complete the pair of the characteristic electrochemical reactions, the electrons generated from the oxidation reactions are utilized in the reduction reaction. In the particular case when the corrosive medium is NaVO3, the expected cathodic reactions could be that whose oxidant species are oxygen and vanadium, such as the next reactions, which also involve chemical reactions [26-28]:

$$VO_3^- + e^- \rightarrow VO_3^{2-} \qquad (7)$$
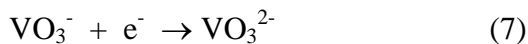
Being VO^{3-} the predominantly vanadium species. This reduction reaction can be followed by a chemical reaction, in which the ion metavanadate VO^{3-} is reversely reduced for producing ions ortovanadates (VO_4^{3-}).

$$VO_3^{2-} + O_2^- \rightarrow VO_4^{3-} + \tfrac{1}{2}O_2 \qquad (8)$$
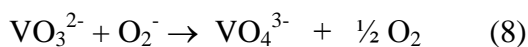
With a subsequent decomposition of the unstable oxyanion species:

$$VO_4^{3-} \rightarrow VO_3^- + O^{2-} \qquad (9)$$
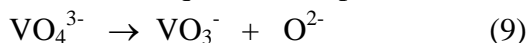
The ion oxygen can be also generated by the next reaction:

$$\tfrac{1}{2}O_2 + 2e^- \rightarrow O^{2-} \qquad (10)$$
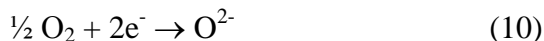
By the other hand, in the outer zone, where the interface metallic oxides/molten salt, the vanadium species is highly concentrated, also observing certain concentration of sodium and oxygen. Apparently, vanadium has not diffused through the oxides to the metallic surface, so, the thick and compact Cr_2O_3 layer and the thin NiO (below the Cr_2O_3 layer) seem to protect AISI-309 after 100 h of exposition from the aggressive and oxidant vanadium. Nevertheless, the dissolution of chromium far away the metallic surface is evident.
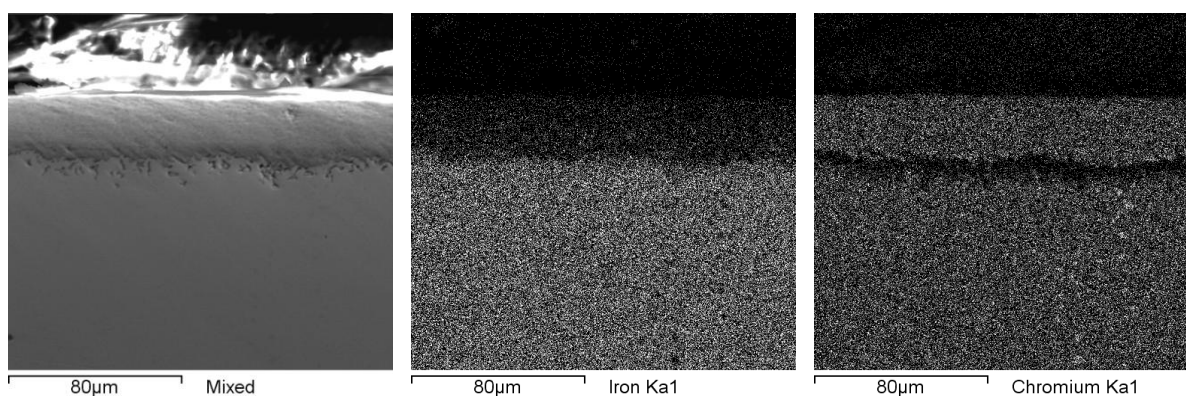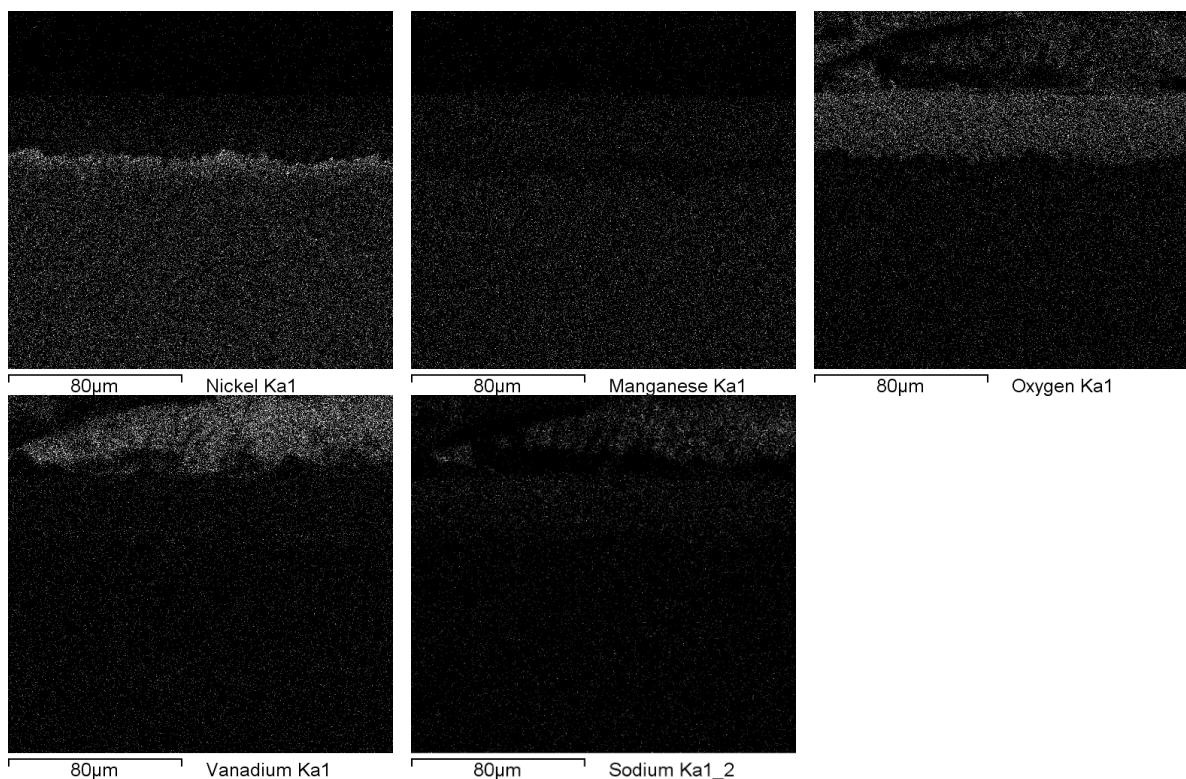
Figure 2. Image of the metal-corrosion products interface and X-ray mappings of Fe, Cr, Ni, Mn, O, V and Na of AISI-310 exposed to $NaVO_3$ at 700°C during 100 h from Lp technique.

Figure 2 presents a micrograph and mappings of Fe, Cr, Ni, Mn, O, V and Na of the substrate-corrosion products interface of the corroded AISI-310 exposed to $NaVO_3$ at 700°C during 100 h from Lp. Such as in the case of AISI-309, from the micrograph of AISI-310, it is possible to see two interfaces: the metallic surface/oxides and the metallic oxides/molten salt. Even though the corrosion mechanism seems to be similar to that for AISI-309, some differences can be observed. The combined oxide layer mainly formed by chromium, iron, and nickel is thinner than that presented for AISI-309, being of 33 μm approximately, however, the concentration of the four individual layers of Cr, Fe, Ni and oxygen are higher. Also, from the micrograph a very dense protective layer is seen over the surface. It is possible that the more defined, thicker and concentrated nickel layer presented just below the Cr_2O_3 layer (in the interface metallic surface-oxides layer) in the case of AISI-310 is due to the major concentration of nickel, but also to the depletion of chromium in the matrix of the material for the marked oxidation suffered for this element, so that, the concentration of nickel is more noticeable. With respect to the mapping of vanadium, it can be seen that it is related with oxygen, chromium and sodium, and in less proportion with iron, so, it is possible to predict the formation of secondary compounds generated from these alloying elements, vanadium, oxygen and sodium.

The corrosion degradation of an alloy depends on its composition, so, it is expected that AISI-310 presents a better corrosion performance. Also, the dissolution of the metallic oxides in any corrosive media is influenced by the characteristics of the oxide layer, such as its density, adherence, thickness, solubility and its growth rate. For instance, the low alloy steels develop oxide layers with high concentration of iron, which are more soluble in sodium vanadates than the oxide layers with high

concentration of chromium formed in austenitic stainless steel [19]. In the particular case of AISI-309 and AISI-310, in general, it was observed the presence of three layers. The outer layer showing the presence of the elements forming the molten salt (V, Na and O), together with chromium and iron, so that, it is possible to presume the presence of porous chromium and iron oxides due to their synergistic dissolution by $NaVO_3$ molten salt. The middle layer is formed by Cr_2O_3, Fe_2O_3 and in less concentration of NiO. The inner layer is formed by a thin and concentrated NiO, especially in the case of AISI-310. Such as it has been discussed in some others works reporting the corrosion in fuel ash, the Cr_2O_3 layer stopped the diffusion of vanadium to the metallic surface, since, it is known that chromium is one of the most resistant elements that increases the corrosion resistant of the materials [29]. In addition, the enrichment of nickel just in the metal-oxide interface observed in alloys with high content of chromium is beneficial, such as presented in both cases of this work, providing that sulfur is not present, otherwise an attack by sulfidation is highly probable [18,19,5].

The presence of vanadium, oxygen and sodium together with the porous chromium and iron oxides in the outer layer leads to anticipate the possible formation of tertiary compounds formed by the fluxing of the corresponding metallic oxides in form of metallic vanadates [30].

Figure 3 shows the corroded specimens of both studied materials obtained from the weight loss method at 100 h, after cleaning from the corrosion products. Both materials were physically characterized using SEM, whereas the corrosion products collected from the cleaning procedure were analyzed by XRD technique, whose spectra are presented in Figures 4 and 5.
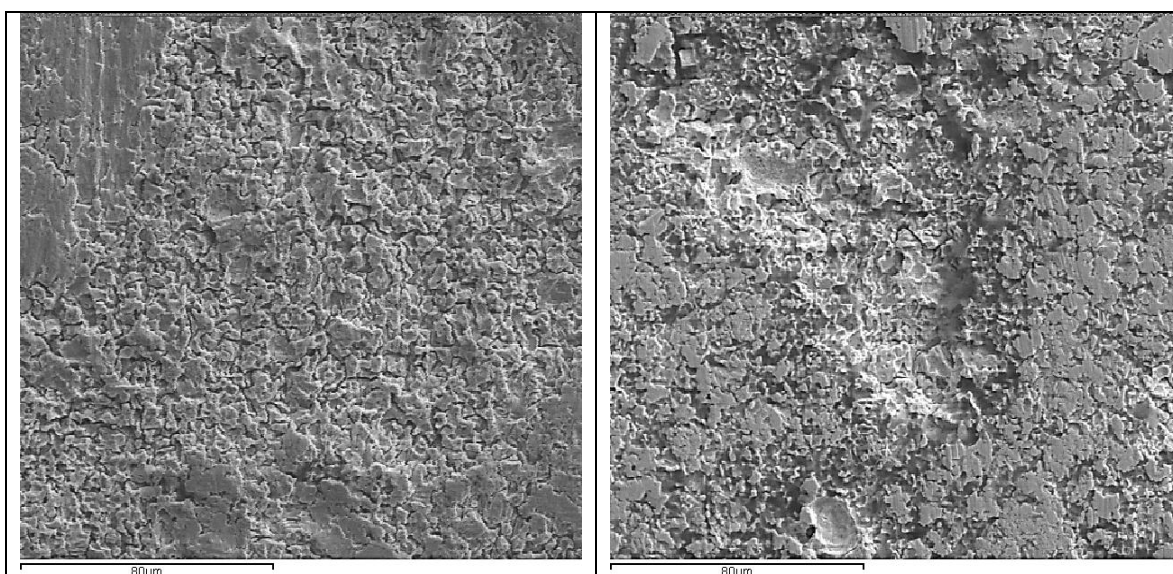

Figure 3. Figure 3. Electron images of AISI-309 free of corrosion products exposing 100 hours to $NaVO_3$ at 700°C at the conventional weight loss method.

These analyses are very important due to the corrosion degradation process is a superficial phenomenon, hence, it is possible to determine the type in which the materials are corroded, making possible to correlate the corrosion type to the mass loss [31]. It is important to mention that a uniform corrosion type is when a site of a material is not more affected than another one, so the active corroded zones are uniformly dispersed over the total surface. On the contrary, a localized corrosion process is

when a particular site is more active than the surface around it. A localized corrosion phenomenon is observed when a material possesses certain intrinsic characteristics (e.g. low corrosion resistance alloying elements), local cracks of the passive layer, metallurgic defects, which promote a local active zone [32]. In some cases a mixed corrosion process has been observed, where uniform and localized events are seen along the surface. From the Figure 3, it is possible to state that both stainless steels presented a similar type of corrosion attack, observing a particular generalized mixed corrosion process throughout the surface: uniform corrosion zones together with localized sites. AISI-310 clearly shows a bigger localized corrosion zone in the middle of the sample. A generalized corrosion process may be due to the synergistic dissolution at different rates of the metallic oxides formed over the surface, which started with a uniform corrosion process, but as time passes, the passivity layer starts to suffer breakdown. At first sight, it would seem that the localized sites draw the grain boundaries; nevertheless, the grains sizes of AISI-309 have been reported elsewhere, lying between 20 μm to 120 μm [19]. By the above described, it is not possible to state that AISI-309 and AISI-310 were attacked by an intergranular corrosion process. By the other hand, although numerous local attacks are seen, this morphology is not the typical of pitting corrosion, in which the passivated material suffers the rupture of the passive film, generating active zones in small areas with high corrosion rates, where the nucleation and subsequent formation of cavities or pits are present [33-35]. Therefore, it seems to be that AISI-309 and AISI-310 were attacked in a localized way probably due to the heterogeneity composition of the passive layer, which was formed by a combination of iron, chromium and nickel oxides, having these elements a different corrosion resistance in molten salts. Also, the formation of those metallic oxides over the surface leads to the depletion of such alloying elements in the matrix of the metal, so, it is possible that such depletion induced the local corrosion sites, such as it is seen in the images. It is important to mention that stainless steel AISI-310 has been evaluated at low temperatures in aqueous bromide solutions, showing a typical pitting corrosion process [36]. At 60°C this material presented pits sized between 270-360 μm, whereas at 80°C the pits lie between 310-370 μm. Additionally, the higher corrosion rate reported for AISI-310 at low temperature (80°C) exposed in bromide aqueous solution was 5.0×10^{-6} g/cm^2, whereas at high temperature (700°C) exposed in NaVO$_3$ was 0.034 g/cm^2, observing a difference of four orders of magnitude. Obviously, the aggressiveness of molten salts at high temperature is enormous.

3.2. X-ray Diffraction Results

Figures 4 presents the XRD spectrum of the scale over the surface of AISI-309 after the exposure in NaVO$_3$ molten salt at 700°C during 100 h, whereas Figure 5 shows the XRD spectrum of the scale of AISI-310 under the same experimental conditions. The corrosion products were obtained from the samples subjected to the weight lost method. The two spectrums indicate the presence of the same compounds: Cr$_2$O$_3$, Fe$_2$O$_3$, FeVO$_4$, CrVO$_4$ and unreacted NaVO$_3$. The elemental analysis from SEM is in agreement with the XRD results. Formation of metallic-V-O compounds was detected as metallic vanadates. Metallic vanadates were obtained from the acidic dissolution of the corresponding stable metallic oxides in presence of the acidic species NaVO$_3$. Such as it has been reported, the ions

vanadates increase the acidic solubility of all the metallic oxides in comparison to pure Na_2SO_4 [37-40], so, the presence of these metallic vanadates was expected. The acidic dissolution of Cr_2O_3, Fe_2O_3 formed when AISI-309 and AISI-310 are exposed to $NaVO_3$ at 700°C can occur accordingly to the next reactions [41-43]:

$$Fe_2O_3 + 2NaVO_3 = 2FeVO_4 + Na_2O \qquad\qquad (11)$$
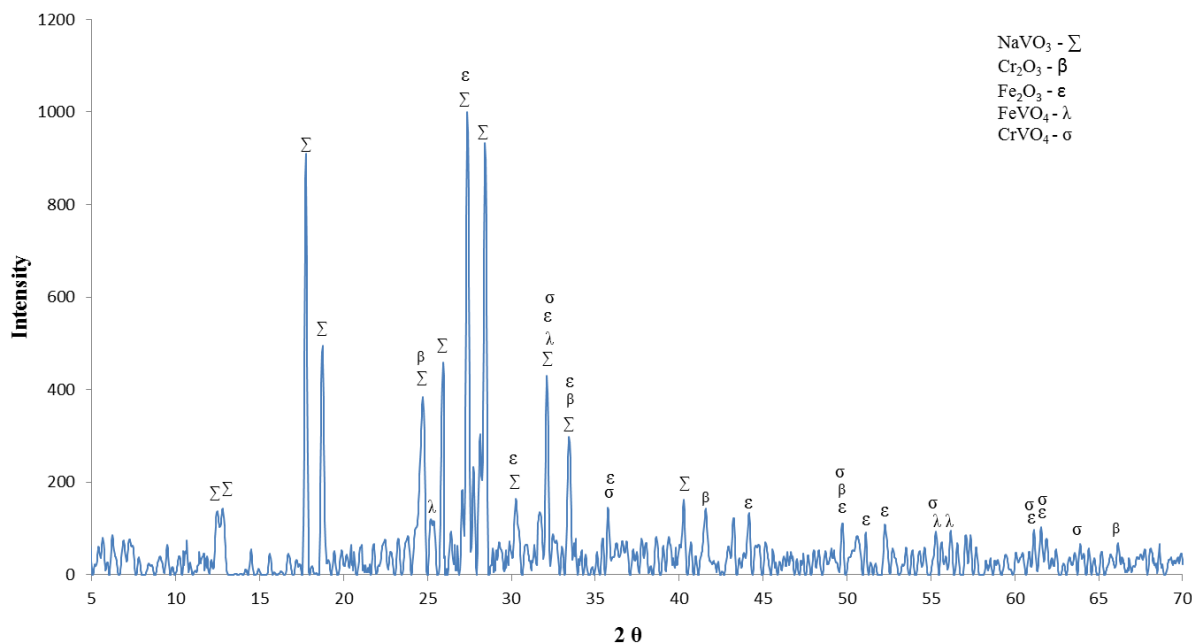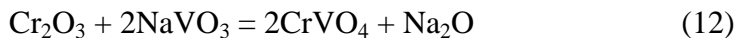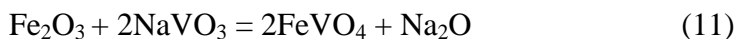$$Cr_2O_3 + 2NaVO_3 = 2CrVO_4 + Na_2O \qquad\qquad (12)$$

Figure 4. XRD analysis of corrosion products formed over the surface of AISI-309 after exposing to $NaVO_3$ at 700°C.
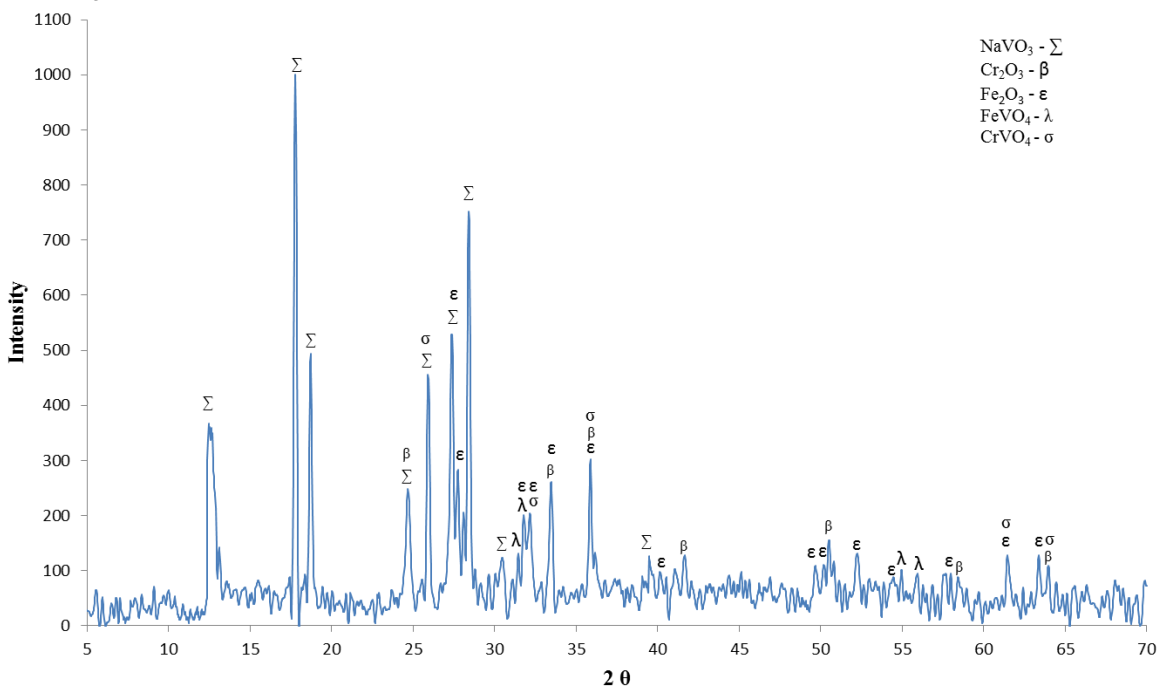

Figure 5. XRD analysis of corrosion products formed over the surface of AISI-310 after exposing to $NaVO_3$ at 700°C.

These chemical reactions represent the acidic dissolution of the two main formed oxides, and they carry out due to the presence of the anion vanadate in the form of $(VO_4)^{-3}$ [41]. In both dissolution reactions, the species vanadium possesses a valence of +5. It is known that depending on the concentration of impurities in the fuel such as V, Na and S, some vanadium compounds as V_2O_5, $NaVO_3$ (sodium metavanadate) and Na_3VO_4 (sodium ortovanadate) can be formed as deposits. The acidity of these three corrosive compounds is major for V_2O_5 and minor for Na_3VO_4, which means that $NaVO_3$ present certain acidity, which must be considered in the proposed corrosion mechanism. In general, vanadates compounds cause a significant increase in the acidity of the melt, increasing the acidic solubility of any metallic oxide; hence, an increase in the dissolution rate is expected.

The species vanadium is a transition element existing in several oxidation states with valences +5 or +4, which are usually the most stables [17,37]. The proportion of vanadium with these valences in the mentioned vanadates constituting the molten salt depends on the partial pressure of O_2 and the basicity of the molten salt. Rapp and col. [37,38,43,44] suggest that the presence of such multivalent ions in the deposits of molten salts can accelerate the corrosion rate, nevertheless, in the present study, it seems that vanadium just exists with one valence (+5). They also determined that the acceleration of the corrosion rate was due to the charge transfer in the molten salts via transition metal ions by counter-diffusion of ions with different valences containing V^{4+} and V^{5+} (for example in melts containing V_2O_4 and V_2O_5); therefore, the transport of the active oxidants in mixtures containing both vanadium compound with two valences must be much faster [17,37]. Given that the species $NaVO_3$ chemically reacts with valence 5+, the expected corrosion rate must be lower than in cases where the species V_2O_5 and V_2O_4 coexist, considering also that the acidity of $NaVO_3$ is lower than that of V_2O_5. Additionally, it is important to observe that in the two dissolution reactions presented in equations 11 and 12, Na_2O is a product; therefore, as the dissolution reactions carried out, the amount of Na_2O in the melt is increased. Na_2O is characterized as a basic compound, which alters the basicity of the melt, so, it can be a controlling factor of the corrosivity of the molten salt, producing a decrease of the acidity in the site where the dissolution reactions are carried out [45].

The contribution of oxygen is evidenced with the presence of metallic oxides, being this species absorbed from the atmosphere. With respect to the transport of oxygen, Wilson [17] indicated that the transport of oxygen through the molten salt can be by ionic movement in a corrosive ionic substance containing mainly the basic species Na_2O, or by means of a more complex mechanism where diffusion assisted by and additional electron transport is present as in semi-conducting molten salts (high vanadium molten salts). In the case of AISI-309 and AISI-310, whose vanadium and sodium mappings show a thick and dense vanadium layer together with a medium concentration thick sodium layer in the outer corrosion zone, and considering an additional amount of sodium due to its formation during the dissolution reactions of the metallic oxides, it is possible to speculate that the oxygen is taken from the atmosphere in then transported by a dual and parallel mechanism, in which a diffusion process is assisted by an electron transport due to the presence of vanadium.

V_2O_5 and sodium vanadates have shown to possess high corrosive characteristics [46]. In addition, it is important to take into account that sodium vanadates are more volatile than Na_2SO_4, and they are a result of a reaction of different compositions between V_2O_5 and Na_2SO_4, such as $NaVO_3$, whose melting point is 630°C, unlike the melting point of V_2O_5 and Na_2SO_4, which are 690 and 884°C

respectively [15,47,48]. Being that the experimental tests were made at 700°C, it is expected that the fluidity of the molten salt be high, which favors the diffusion and the interaction of active species during the corrosion process, therefore, the electrochemical and chemical reactions are expected to carry out faster.

Nevertheless, the possible corrosion products as primary, secondary and tertiary compounds formed through the electrochemical and chemical reactions have higher melting points than pure $NaVO_3$ (see Table 2). Such fact leads to a reduction of the corrosion of the molten salt [49], due to the reduction of the fluidity of the initially pure $NaVO_3$ [6,48]. For the above analysis of the possible corrosion mechanism, it is possible to speculate that in the extend that the formation and accumulation of metallic vanadates as corrosion products together with $NaVO_3$, the corrosion rate of AISI-309 and AISI-310 could be decreased in time.

Table 2. Melting points of some corrosion products.

Corrosion Products	P. F. (°C)
$FeVO_4$	760
$CrVO_4$	810

3.3. Electrochemical Characterization

3.3.1. Potentiodynamic Polarization Measurements

Figure 6 shows the potentiodynamic polarization measurements (PM) for the two studied materials exposed to $NaVO_3$ at 700°C. From the polarization measurements, the corrosion rate at stable state was obtained applying the Tafel extrapolation method, also in some cases, some aspects of the corrosion mechanisms may be also determined. From the PC´s it is stated that the free corrosion potentials E_{corr} of AISI-309 and AISI-310 are very similar: -171 mV and -163 mV respectively. By the other hand, the current density corrosion i_{corr} obtained from the Tafel extrapolation shows a higher value for AISI-309, 2.63 mA/cm^2, compared to that for AISI-310, which was 1.2 mA/cm^2. The more active potential (more negative) and the higher current density make to assume the formation of less protective corrosion products [50].
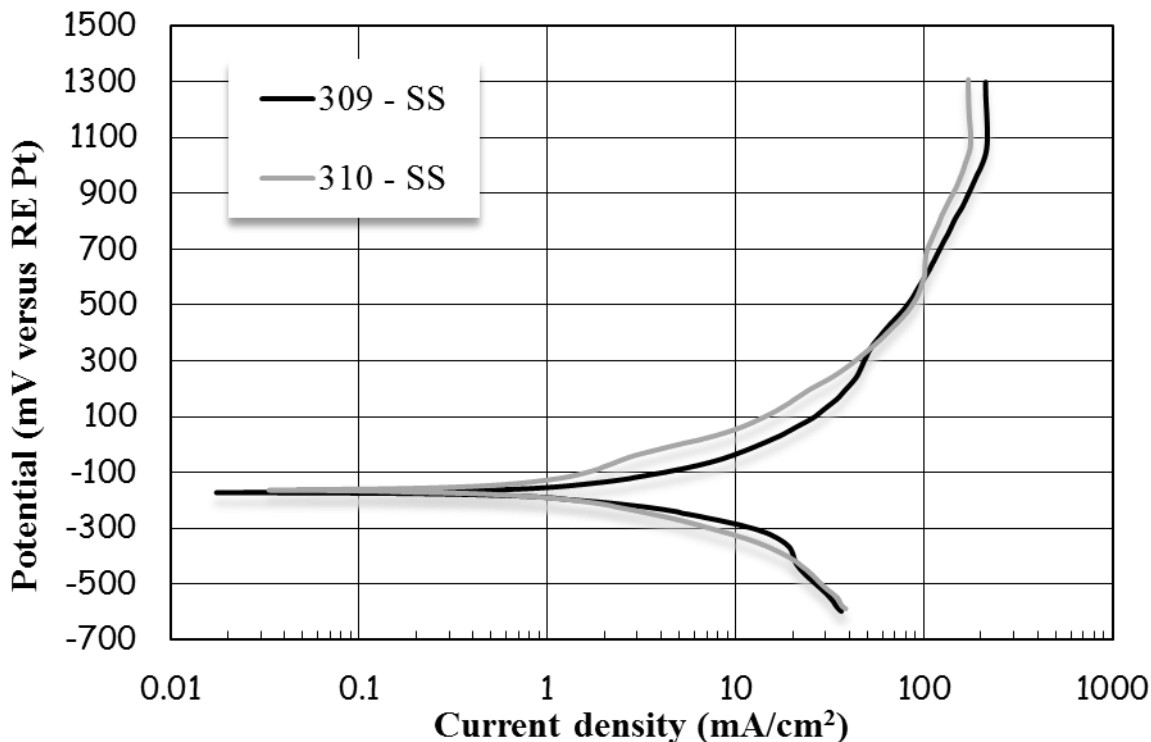
Figure 6. Polarization curve for AISI-309 and AISI-310 exposed to $NaVO_3$ at 700°C.

After using the Tafel method, the anodic and cathodic Tafel slopes were over 100 mV/dec, indicating the importance of diffusion processes, especially in the case of AISI-309, where the Tafel slopes were the largest values (See Table 3). The diffusion of some species can have a significant effect on the rate controlling step, and when Tafel slopes are not lower than 100 mV/dec, the corrosive systems are not purely charge transfer or diffusion controlled [51,52]. This behavior can be due to the fact that $NaVO_3$ containing the species vanadium is considered a semi-conducting molten salt, nevertheless during the dissolution reactions of the several metallic oxides the basic species Na_2O is formed, whose transport if considered by ionic movement, therefore, it is possible to expect a combined mechanism in which the transport of mass species and electrons have and important role.

Table 3. Electrochemical parameters obtained from the potentiodynamic polarization measurements for AISI-309 and AISI-310.

Materials	E_{corr} (mV)	i_{corr} (mA/cm^2)	β_a	β_c
309	-171	2.63	238	191
310	-163	0.76	191	128

The behavior of the anodic branch shows that the corrosion phenomenon was almost active along the applied potential, which indicates a constant dissolution of the metallic oxides, observing the

absence of passivity, however, the last portion of the curve (from 1100 to 1300 mV) of AISI-309 presents a limit current at 213 mA/cm^2 approximately. With respect to AISI-310, the same limit current was observed at a smaller current density (170 mA/cm^2), but a second limit current was also seen between 620 to 700 mV, having a current density of 100 mA/cm^2. While it is true that a passivation should show a decrease of the current density, indicating the protectiveness of the metallic oxides, it is also true that a constant current shows the evidence that the metallic oxides are restraining an increase of the corrosion rate, considering that the metallic oxides have certain protective characteristics. Considering the qualitative behavior of both PC´s, it can be said that the two materials had a similar corrosion mechanism, such as it was observed from the mappings and DRX analyses. The little difference in the best corrosion performance of AISI-310 given by its nobler E$_{corr}$, its smaller i$_{corr}$ and also a smaller limit current at the major potentials may be due to its slight higher composition in chromium and nickel. The chromium oxide as a dense and adherent layer over the surface and the well define thin and dense nickel oxide layer below the chromium oxide layer were the responsible to protect the material. Until now, it can be stated that AISI-309 and AISI-310 suffered a similar corrosion attack: uniform corrosion at the beginning of the exposure, then, the depletion of some elements was obvious due to oxidation and later dissolution of the alloying elements (especially for chromium), so, the localized corrosion was carried out in a generalized way, not evidencing a pitting or intergranular corrosion [53].

3.3.2. Linear Polarization Resistance

Utilizing the analyzer program of the Potentiostat/Galvanostat, which uses an algorithm of the Tafle method, Tafel slopes were obtained from the potentiodynamic polarization measurements, and then the constant B of the equation 2 was calculated in order to be utilized in the Stern-Geary equation (Eq. 2) such as has been reported elsewhere [19,24,54,55].

$$I_{corr} = \frac{B}{Rp} \qquad \text{Eq. [1]}$$

$$B = \frac{b_a b_c}{2.303(b_a + b_c)} \qquad \text{Eq. [2]}$$
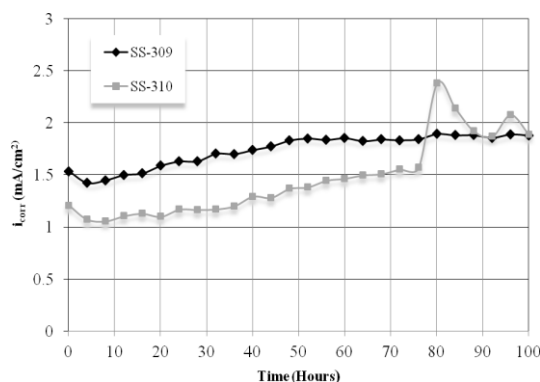

Figure 7. Icorr from the linear polarization resistance for AISI-309 and AISI-310 exposed to NaVO$_3$ at 700°C.

Figure 7 presents current density corrosion obtained from the linear polarization resistance electrochemical technique for AISI-309 and AISI-310 exposed to NaVO₃ at 700°C. From this technique, the corrosion rate in time was obtained [32]. Additionally, due to the polarization is very small with respect to the corrosion potential (±10 mV), such perturbation does not affect significantly the corrosion process, so, the corrosion process is considered as free corrosion, and hence, this technique can be used for a long time, provided that a catastrophic corrosion was not present [37, 56].

From Figure 7, it is evidenced that AISI-310 has a better performance until the 77 h with respect to AISI-310, observing some oscillations at the rest of the test time, nevertheless at the last 12 h, the tendency was to keep constant. It is probable that this behavior was presented due to the major depletion of chromium, which was clearly seen in the image of Figure 2 of the AISI-310, such depletion is encouraged by the loss of atoms, which are ionized during the oxidation reactions producing an increase of the current density corrosion. In order to corroborate the results obtained from the linear polarization resistance technique, the potential was measured during the same time, whose results are shown in Figure 8. From this result, it is seen that AISI-310 presented the nobler potentials along the test, observing a decrease around 80 h, which is in agreement with the icorr presented above. Lower potentials would indicate that AISI-310 is less electrochemically active. Nevertheless, it is noticed that the current density corrosion values of both materials are very similar, observing the same trend.
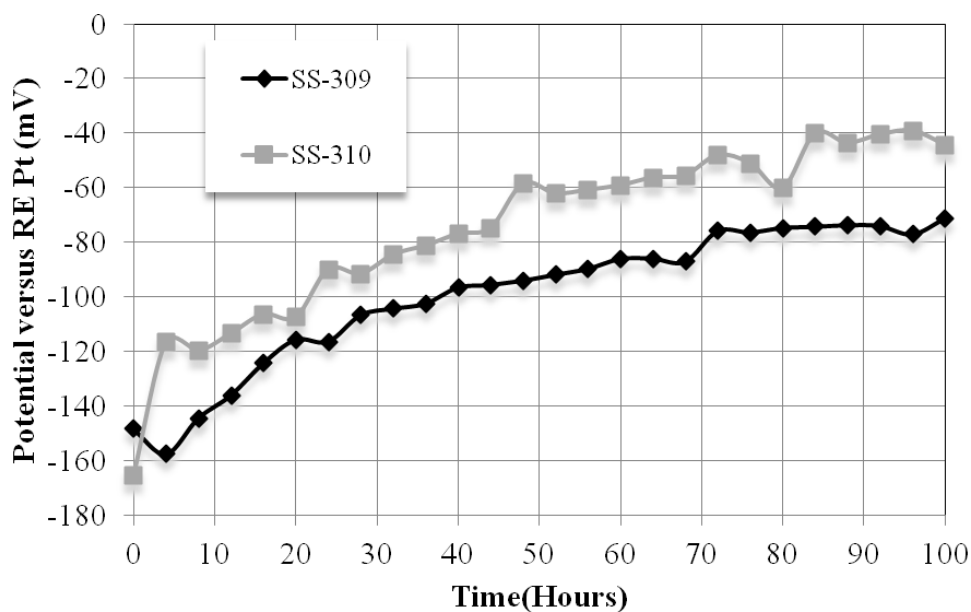

Figure 8. Potential obtained in free corrosion for AISI-309 and AISI-310 exposed to NaVO₃ at 700°C.

For the purpose of exploring the further performance of AISI-309 and AISI-310, the conventional weight loss method was used for 250 h under the same experimental conditions, whose results each 50 h are presented in Figure 9. From the WL method, it is observed that the weight loss behavior of both materials is similar from the quantitative and qualitative way, being in the same order

of magnitude in a range of 0.0125 to 0.033 mg/cm^2. In this case, the corrosion rate resulted lightly major for AISI-310, which is not at all congruent with that obtained from the electrochemical techniques. It is important to note that the results from the conventional weigh loss method can have some errors, especially due to the risk in the cleaning process, mostly when the corrosive medium is molten salts at high temperatures. The generalized mixed corrosion suffered by both materials (in which there are many small depletion sites and uniform corrosion zones along the surface) represents a difficult for cleaning the samples, through which an underestimation or overestimation of mass loss may occur. Also, the measurements of the mass loss must be taken through a more or less long time in order to obtain assessable data, in this case, data were taken each 50 h, which means that detailed mass loss information is not available, therefore, this fact represents a disadvantage of the weight loss method compared to the electrochemical techniques. So, in conclusion, from the qualitative and quantitative point of view AISI-309 and AISI-310 have presented a similar way to be corrosive attacked by NaVO$_3$ at 700°C, and the small difference in composition seems not have a relevant significance in the corrosion mechanism presented for these two alloys. So, the electrochemical and weigh loss data obtained in this study have provided interesting and reliable information in the determination of the corrosion type, the corrosion rate and some aspects of the corrosion mechanism.
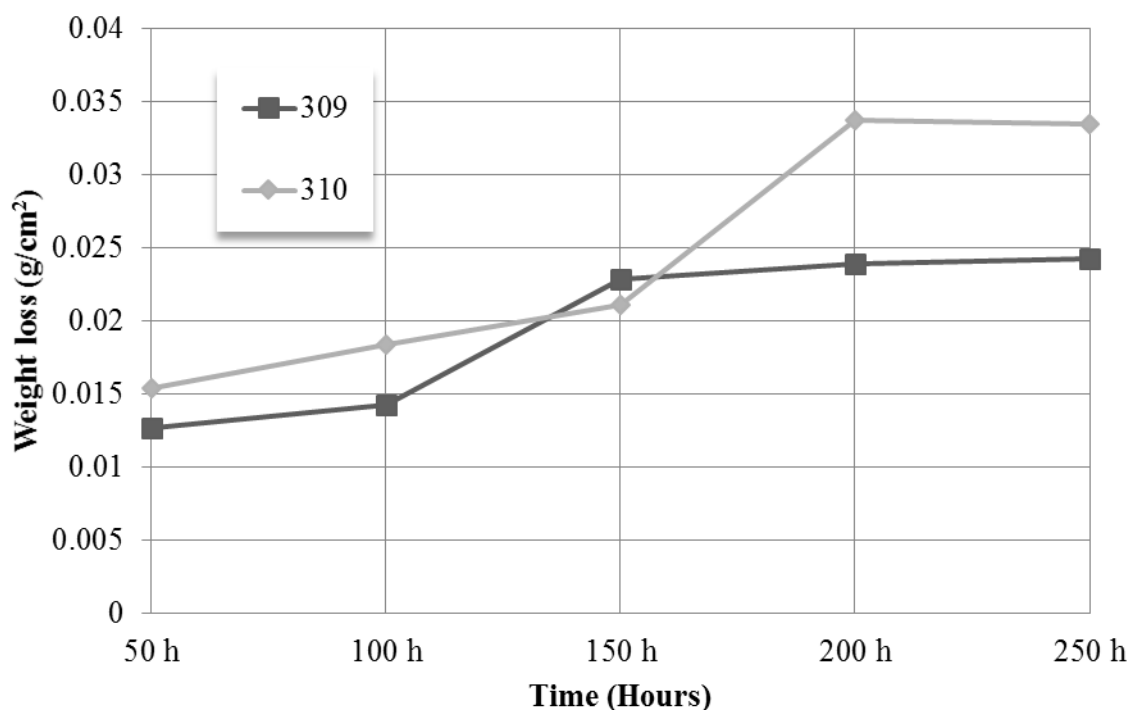

Figure 9. Mass loss along 250 h obtained from the conventional weight loss method for AISI-309 and AISI-310 exposed to NaVO$_3$ at 700°C.

4. CONCLUSIONS

From the physical characterization of the corroded AISI-309 and AISI-310 and the electrochemical tests together with the mass loss data, it is possible to state the next conclusions when these two stainless steels were exposed to NaVO$_3$ molten salt at 700°C.

During the corrosion process AISI-309 and AISI-310 formed two interfaces: the metallic surface/oxides and the metallic oxides/molten salt. The mappings of Fe, Cr and Ni showed the presence of a chromium, iron and nickel (the last one in much lesser extent) layer related with oxygen, for AISI-309, 40 μm thickness; whereas for AISI-310, 33 μm thickness. This layer was denser and more coherent for AISI-310. Below this dense layer, there was a 4 μm thin nickel layer for both materials, which was just in the interface metallic surface/oxides. This thin nickel layer was non-continuous and less dense for AISI-309. The chemical and electrochemical reactions presented in this work were suggested for the corrosion mechanism of both materials, evidencing the presence of Cr_2O_3 and Fe_2O_3 as the main formed oxides and $FeVO_4$ and $CrVO_4$ as the secondary compounds, which contribute to decrease the fluidity of the melt in time, expecting a reduction of the corrosion rate. From the dissolution reactions, the formation of Na_2O is evident, which leads to a decrease of the solubility of the metallic oxides, also contributing to a decrease of the corrosion activity. Both stainless steels presented a similar type of corrosion attack, observing a particular generalized mixed corrosion process throughout the surface: uniform corrosion zones together with localized sites.

From the electrochemical techniques it was determined that AISI-310 has a better corrosion performance respect to AISI-309, since its corrosion potential was nobler and the current density corrosion was smaller. Nevertheless, the data of both materials were alike, being in the same order of magnitude. From the qualitative and quantitative point of view, AISI-309 and AISI-310 have presented a similar way to be corrosive attacked by $NaVO_3$ at 700°C, and the small difference in composition seems not have a relevant significance in the corrosion mechanism. So, the electrochemical and weigh loss data obtained in this study have provided interesting and reliable information in order to evaluate the probable use of these stainless steels in applications where the fuel in industrial furnaces is a residual oil containing the species vanadium.

References

1. Harpreet Singh, Devendra Puri and Satya Prakash, *Rev. Adv. Mater. Sci.*, 32 (2007) 1627
2. Bryers W. Richard, *Energy Combust. Sci.*, 22 (1996) 120
3. W. D. Halstead, *J. Inst. Fuel*, 45 (1970) 234
4. A. Wong-Moreno, R.I. Marchan Salgado, Molten salt corrosion of heat resisting alloys, in: CORROSION 95, NACE International, Houston TX, Paper 465, 1995.
5. C. Cuevas-Arteaga, J. Uruchurtu-Chavarín, J. Porcayo-Calderon, G. Izquierdo, J. González, *Corros. Sci.*, 46 (2004) 2663
6. G. W. Cunningham and A. S. Brasunas, *Corrosion*, 12 (1956) 35
7. S. A Shchukarev, G. A. Semenov and K. E. Frantseva, *Russ. J. Inorg. Chem.*, 11 (1966) 129.
8. S. Killingbeck, Vaporization of vanadium oxide. Thermodinamic and phase studies, University of Kansas, Ph.D. Thesis, Department of Chemistry, 1964
9. A. S. Kallend, *Combust. flame*, 11 (1967) 81
10. E. F. Milan, *J. Phys. Chem.*, 33 (1929) 498

11. D. A. Pantony and K. I. Vasu, Thermodynamics and kinetics in molten vanadium pentoxide. Proc. of the First International Thermal Analysis Conference. Aberdden ED. J. P. Redfearn, MacMillan and Co., Ltd., London, Paper 168, 1965

12. N. P. Allen, O. Kubaschewski and O. J. Von Goldbeck. *J. Electrochem. Soc.*, 98 (1951) 417

13. N. D. Philips and C. L. Wagoner, Oil ash corrosion of superheater alloys in a pilot scale furnace-reduction by use of additives, ASME Annual Meeting, Atlantic City, N.J., November 29-December 4, 1959.

14. K. H. Brinsmead and R. W. Kear, *Fuel,* 35 (1965) 84

15. Alexander A. Patricia and Marsden A. Ruth., Corrosion of Superheater Materials by Residual Oil Ash, Proceedings of the Marchwood Conference, Mechanism of Corrosion by Fuel Impurities, edited by Johnston and Littler, Butterworths, London, 542-555, 1963

16. E. Otero, A. Pardo, J. Hernaez, and P. Hierro, *Reviews in Metal Madrid*, 1 (1990) 26

17. J.R. Wilson, Understanding and preventing fuel ash corrosion, in: CORROSION/76, NACE International, 1976, pp. 12/1–12/23.

18. A. Wong-Moreno, Y. Mujica Martinez, L. Martınez, High Temperature Corrosion enhanced by Residual Fuel Oil Ash Deposits, CORROSION/94, NACE International, Paper 185, 1994.

19. C. Cuevas-Arteaga, *Int. J. Electrochem. Sci.*, 7 (2012) 12283

20. ASTM Standard G1: Practice for Preparing, Cleaning, and Evaluating Corrosion Test Specimens, 1994.

21. ASTM Standard G31: Practice for Laboratory Immersion Corrosion Testing of Metals, 1995.

22. L. G. Berry, Powder Diffraction Data File. – Inorganic phases. Publication of the joint committee on powder diffraction standards.

23. Kari Korpiola, High Temperature Oxidation of Metal, Alloy and Cermet Powders in HVOF Spraying Process, Doctoral Thesis, Helsinki University of Technology Publication in Materials Science and Metallurgy, 2004.

24. O. Sotelo-Mazón, C. Cuevas-Arteaga, J. Porcayo-Calderón, V.M. Salinas Bravo, G. Izquierdo-Montalvo, *Adv. Mater. Sci. Eng.*, (2014) Article ID 923271, 12.

25. C. Cuevas Arteaga, J. Porcayo Calderón, C. F. Campos Sedano, J. A. Rodríguez, *Int. J. Electrochem. Sci.,* 7 (2012) 445

26. D. Z. Shi, J. C. Nava, and R.A. Rapp, Electrochemical reactions by $NaVO_3$ and Na_2CrO_4 solutes in fused Na_2SO_4, High Temperature Materials Chemistry, IV Conference, Electrochemical American Society, USA, 1987.

27. C. Cuevas Arteaga, J. Porcayo Calderon, G. Izquierdo, A. Martinez Villafañe and J.G. Gonzales Rodriguez, *Mater. Sci. Tech.-Lond.*, 17 (2001) 216

28. J. Pan, C. Leygraf, R. F. A. Jargelius-Pettersson and J. Linden, *Oxid. Met.*, 50 (1998) 177

29. E. Mohammadi Zahrani, and A.M. Alfantazi, *Corros. Sci.* 65 (2012) 340

30. A. Wong-Moreno, R.I. Marchán Salgado, L. Martínez, "Molten Salt Corrosion of heat resisting alloys", CORROSION/95 (NACE International), Paper 465, pp. 465/1-465/16, (1995).

31. C. Cuevas-Arteaga, J. Porcayo-Calderon, G. Izquierdo-Montalvo, G. Gonzales-Rodríguez, *Rev. Mex. Ing. Quim.* 2 (2003) 135

32. Ellor A. James, Uniform, Corrosion test and standard manual application and Interpretation; Ed. ASTM Manual series, USA, 1995.

33. Robert Baboian, Sheldon Dean, Harvey Hack, Gardner Haynes, John Scully, Donald O. Sprowls, Corrosion Tests and Standards: Application and Interpretation, in: Robert Baboian (ed.), ASTM Manual Series MNL20, Electrochemical, Philadelphia PA, USA, 1995, 75-90.

34. C. Cuevas Arteaga, *Rev. Mex. Ing. Quím.,* 5 (2006) 27

35. C. Cuevas-Arteaga, J. Porcayo-Calderón, *Mat. Sci. Eng. A*, 435 (2006) 439

36. C. Cuevas Arteaga, M. Luna Brito, A. Molina-Ocampo, J. Colín, S. Serna-Barquera, A. Torres-Islas, *Int. J. Electrochem. Sci.*, 8 (2013) 9593

37. X. Zheng and Robert A. Rapp, *J. Electrochem. Soc.*, 142-1 (1995) 142

38. Y.S. Hwang and R.A. Rapp, *Corrosion*, 45 (1989) 933
39. Robert A. Rapp and Y. S. Zhang, Electrochemical studies of hot corrosion of materials, Proceedings of the First Mexican Symposium on Metallic Corrosion, Paper 12, pp. 90-99, México (1994).
40. Robert A. Rapp, *High Temper. Sci.*, 27 (1990) 355
41. Robert A. Rapp, *Mater. Sci. Eng.*, 12 (1987) 319
42. Y. S. Zhang and Robert A. Rapp, Solubility of CeO_2 in molten Na_2SO_4-10% mol $NaVO_3$ salt solution at 900°C", Proceedings of the Ninth International Symposium on Molten Salts" Electrochemical Society, 1994.
43. Robert Rapp, K.S. Goto, The hot corrosion of metals by molten salts". Conference Proccedings 2nd. International Symposium on Molten Salts, New Jersey, USA, Electrochemical Society, 159-177, 1981.
44. N. Otsuka and R. Rapp, *J. Electrochem. Soc.*, 137 (1990) 53
45. L. D. Paul and R.R. Seeley, Oil ash corrosion - A review of utility boiler experience, CORROSION/90 (NACE International), paper 267, pp. 267/1-267/15 (1990).
46. D.A. Pantony and K.I. Vasu, *J. Inorg. Nucl. Chem.*, 30 (1967) 423
47. Y. Harada, S. Naito, T. Tsuchiya, Y. Nakajima. "Problems of low grade oil firing boilers and their solutions", Mitsubishi technical bulletin (1981) 85
48. H. Lewis, *Brit. Petrol. Equip. News,* 7-17 (1957) 23
49. E. Rocca, L. Aranda, M. Moliere, and P. Steinmetz, *J. Mater. Chem.*, 12 (2002) 3766
50. C. Cuevas-Arteaga, J. Uruchurtu-Chavarín, J. González, G. Izquierdo-Montalvo, J. Porcayo-Calderón, and U. Cano-Castillo, *Corrosion*, 60 (2004) 548
51. C. Cuevas Arteaga, *Corros. Sci.*, 50, (2008) 650
52. K. Skinner, J. *Br. Corros.*, 22 (1987) 172
53. Handbook of Corrosion Engineering; Pierre R. Roberge; Edit; MacGraw-Hill; USA; 2000.
54. X.Y. Zhou, S.N. Lvov, X.J. Wei, L.G. Benning, D.D. Macdonald, *Corros, Sci.*, 44 (2002) 841
55. J Porcayo-Calderón, C.D. Arrieta-González, A. Luna-Ramírez, V. M. Salina-Bravo, C. Cuevas-Arteaga, A. Bedolla-Jacuiende and L. Martínez-Gómez, *Int. J. Electrochem. Sci.*, 8 (2013) 12205
56. U.K. Chatterjee, S. K. Bose, S.K. Roy, *Environmental degradation of metals*, Marced Dekker, Inc. New York, (2001).